JOURNAL OF MATERIALS SCIENCE 30 (1995) 2194–2200

Phase transformation and microstructural changes of Si_3N_4 during sintering

Y. GOTO*, G. THOMAS
National Center for Electron Microscopy, Lawrence Berkeley Laboratory, and Department of Materials Science, University of California, Berkeley, CA 94720, USA

Changes of density, the α–β phase transformation, and composition of grains and grain boundaries during sintering of Si_3N_4 with various sintering conditions using additives of Y_2O_3 and Al_2O_3 were investigated. The phase determination of individual Si_3N_4 grains was performed by convergent beam electron diffraction. The relations between densification and transformation were divided into two groups, depending on the additive compositions. Aluminium dissolution into Si_3N_4 grains occurred mostly during α–β transformation process. The concentrations of aluminium and oxygen in the grain boundaries decreased as the α–β transformation progressed.

1. Introduction

Increasing attention is being directed toward Si_3N_4 ceramics for structural applications at high temperature because of their high resistance to thermal shock, together with high strength, good fracture toughness, and high resistance to chemical attack. Mechanical properties depend on microstructure, which is dependent on the sintering history and composition of additives. Recently, the mechanical properties of Si_3N_4 have been improved greatly and extensive efforts have been made by many investigators. However, further improvement is still required for applications at extremely high temperature, such as for gas turbine parts [1].

There are numerous complicated changes in the heating process of Si_3N_4, including densification, transformation of α- to β-Si_3N_4, grain growth, aluminium dissolution into the Si_3N_4 grains which forms the β′-phase, and grain-boundary composition changes. In spite of much research on the microstructure and sintering behaviour (e.g. [2–4]), the identification of these relationships is still not clear; for example, the relations between aluminium dissolution, transformation, and grain-boundary composition changes. Grain-boundary composition has been linked to high-temperature strength and oxidation resistance [5–8].

It is believed that high strength and high fracture toughness of Si_3N_4 ceramics are brought about by a microstructure characterized by elongated β-Si_3N_4 grains which are closely entangled and linked together [9]. This microstructure is closely related to the α–β transformation and densification. Aluminium dissolution into Si_3N_4 grains affects the elongation of β-Si_3N_4 grains.

In order to clarify further the structural, microstructural, and compositional changes during sintering of Si_3N_4, the present study by X-ray diffraction and electron optical methods was undertaken, with special emphasis placed on microdiffraction by convergent beam electron diffraction (CBED) and microanalysis. Attention was focused on the α–β transformation and compositional changes in Si_3N_4 grains and at grain boundaries. Thus, samples from various stages of the sintering process were used, and the phase and composition of grains and grain boundaries were analysed.

2. Experimental procedures

2.1. Material fabrication

The starting powders were prepared by ball-mill mixing a commercial grade Si_3N_4 powder (E-10, Ube Industry Co. Ltd., Tokyo, Japan) with various composition of Al_2O_3 and Y_2O_3 powders as sintering additives for 24 h, using *n*-butanol as a liquid medium. The additive compositions are listed in Table I. The notations of additive composition in Table I are used in the remainder of this paper. After drying, the powders were cold-pressed at the pressure of 60 MPa to shape the green compacts of 18 mm diameter and 9 mm thick. Hot-pressing was done in a carbon die at temperatures of 1550–1800 °C and at a pressure of 40 MPa with no holding time under 0.1 MPa N_2. The heating rate was 17 °C min^{-1}. After the prescribed temperatures were reached, the samples were rapidly cooled by heater shutdown and by removal of samples from the heating zone to a cooling zone where cold nitrogen gas was flowing, in order to suppress significant changes from occurring in the samples during cooling. To complete densification, one sample for each composition was hot-pressed at 1800 °C for 60 min.

* *Present address*: Research and Development Center, Toshiba Corporation, 1, Komukai Toshiba-cho, Saiwai-ku, Kawasaki, 210, Japan

0022–2461

TABLE I Additive composition (wt %)

	Y_2O_3	Al_2O_3
10A	0	10
1Y6A	1	6
3Y4A	3	4
5Y2A	5	2

2.2. Microstructural characterization

The density and β-Si_3N_4 content were measured for each sample. The density was determined by measurements of shrinkage and weight. In assessing the density achieved during hot-pressing, the relative density was calculated based on the assumption that the density of the sample hot-pressed at 1800 °C for 60 min was the full density. The β-phase content was measured by X-ray diffraction using CuK_α radiation. The β-phase concentration in Si_3N_4 was derived from the X-ray intensities of (1 0 2) and (2 1 0) reflections of α-Si_3N_4 and (1 0 1) and (2 1 0) reflections of β-Si_3N_4 [10].

Selected specimens were examined by transmission electron microscopy (TEM) and energy dispersive X-ray spectroscopy (EDS). Specimens were prepared from Si_3N_4 samples by ion-beam thinning to achieve electron transparency. A thin layer of carbon was then evaporated on to the specimen to minimize charging under the electron beam. Microstructures of the Si_3N_4 samples were examined in a 120 kV TEM (Model 400T, Philips Gloeilampenfabrieken NV, Eindhoven, The Netherlands) using conventional techniques of bright- and dark-field imaging and diffraction. Analytical electron microscopy was performed on a 200 kV instrument (Model JEM-200CX, JEOL Corp., Foster City, CA) equipped with an ultra-thin-window spectrometer (Model Microanalyst-8000, Kevex Corp., Foster City CA), allowing detection of elements having atomic number ≥ 5. The Cliff–Lorimer k factors were determined experimentally for the analytical microscope used in this study [11].

The crystalline phases of each Si_3N_4 grain were identified by microdiffraction using the CBED technique [12–14], which allows identification of both α and β phases. These phases are hexagonal modifications, with lattice parameters along the a-axis being almost the same, but the c-parameter of α-Si_3N_4 is above twice as large as that for the β-modification [2]. Thus, differences in higher-order Laue zone ring spacings allow for rapid identification. Only in special cases (orientations) can selected-area electron diffraction (SAD) distinguish between these phases, but with much poorer spatial resolution than is possible with CBED (~2 nm).

3. Results and discussion

3.1. Densification and transformation

The relative densities and β-Si_3N_4 content as a function of sintering temperature are shown in Figs 1 and 2, respectively. Both the densification and transformation rates are dependent on the additive composition. The 1Y6A additive had the highest densification rate

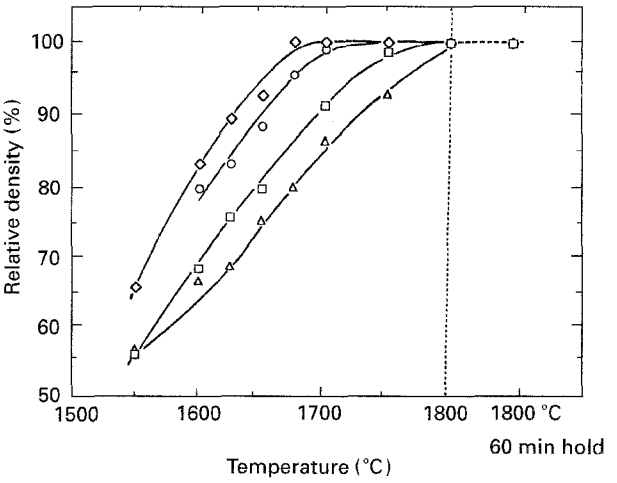

Figure 1 Variation of relative density with sintering temperature for various additive compositions: (□) 10A, (◇) 1Y6A, (○) 3Y4A, (△) 5Y2A.

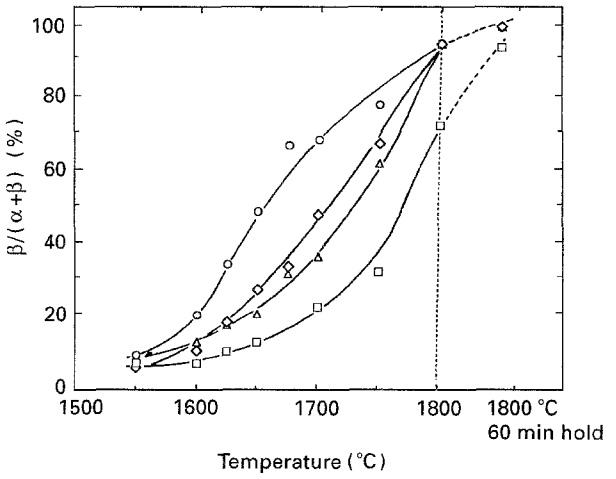

Figure 2 Variation of β-Si_3N_4 content with sintering temperature for various additive compositions: (□) 10A, (◇)1Y6A, (○) 3Y4A, (△) 5Y2A.

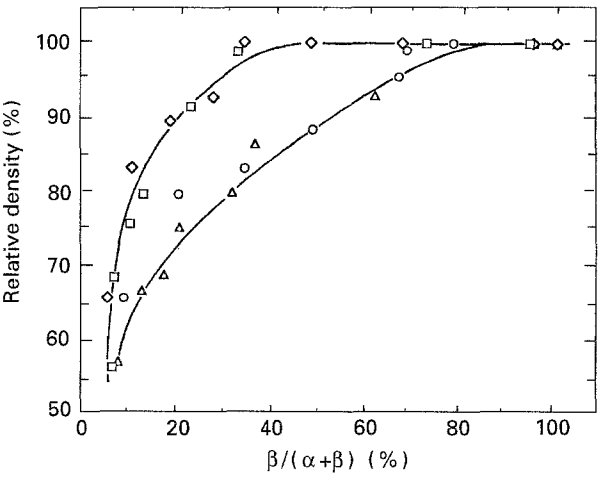

Figure 3 Variation of relative density with β-Si_3N_4 content for various additive compositions: (□) 10A, (◇) 1Y6A, (○) 3Y4A, (△) 5Y2A.

while the 3Y4A additive and the highest transformation rate. To examine the relation between densification and transformation, both sets of data can be compared, as shown in Fig. 3. This plot reveals that

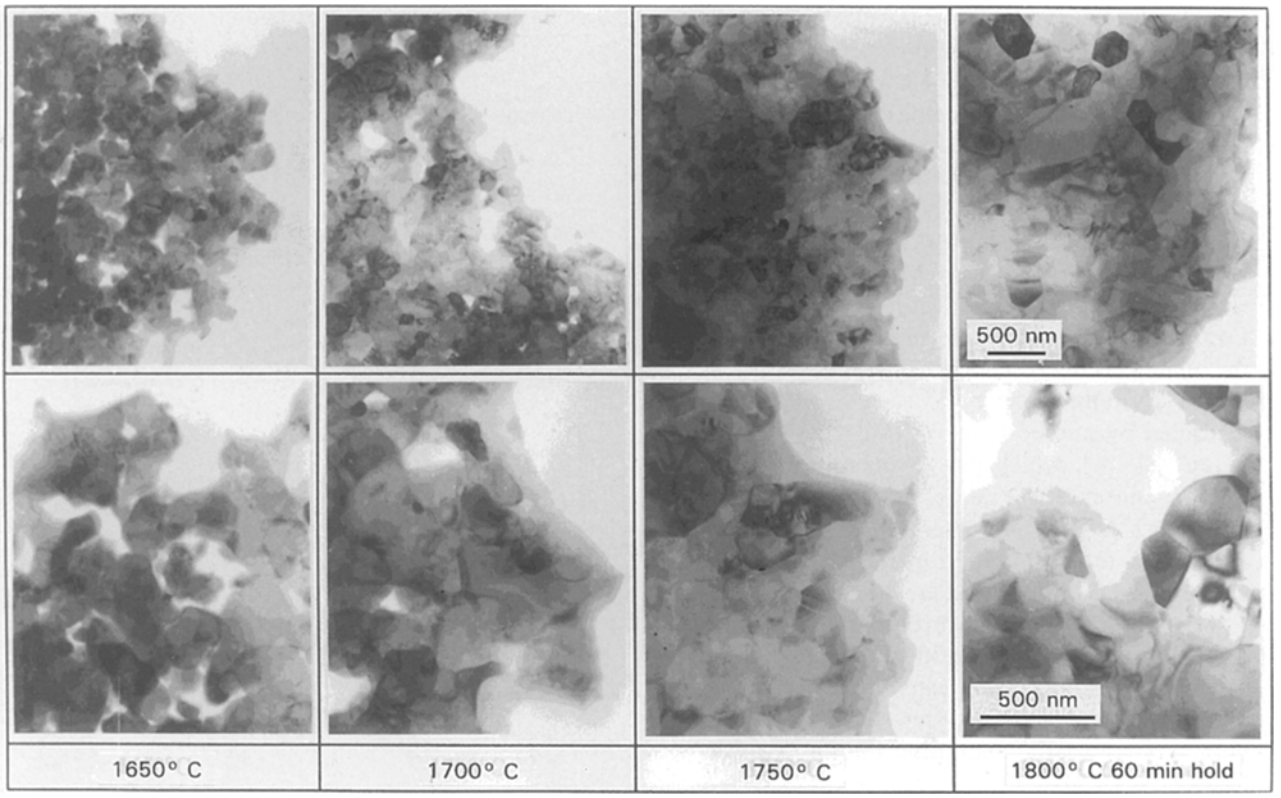

Figure 4 Transmission electron micrographs of Si_3N_4 with 5% Y_2O_3 and 2% Al_2O_3.

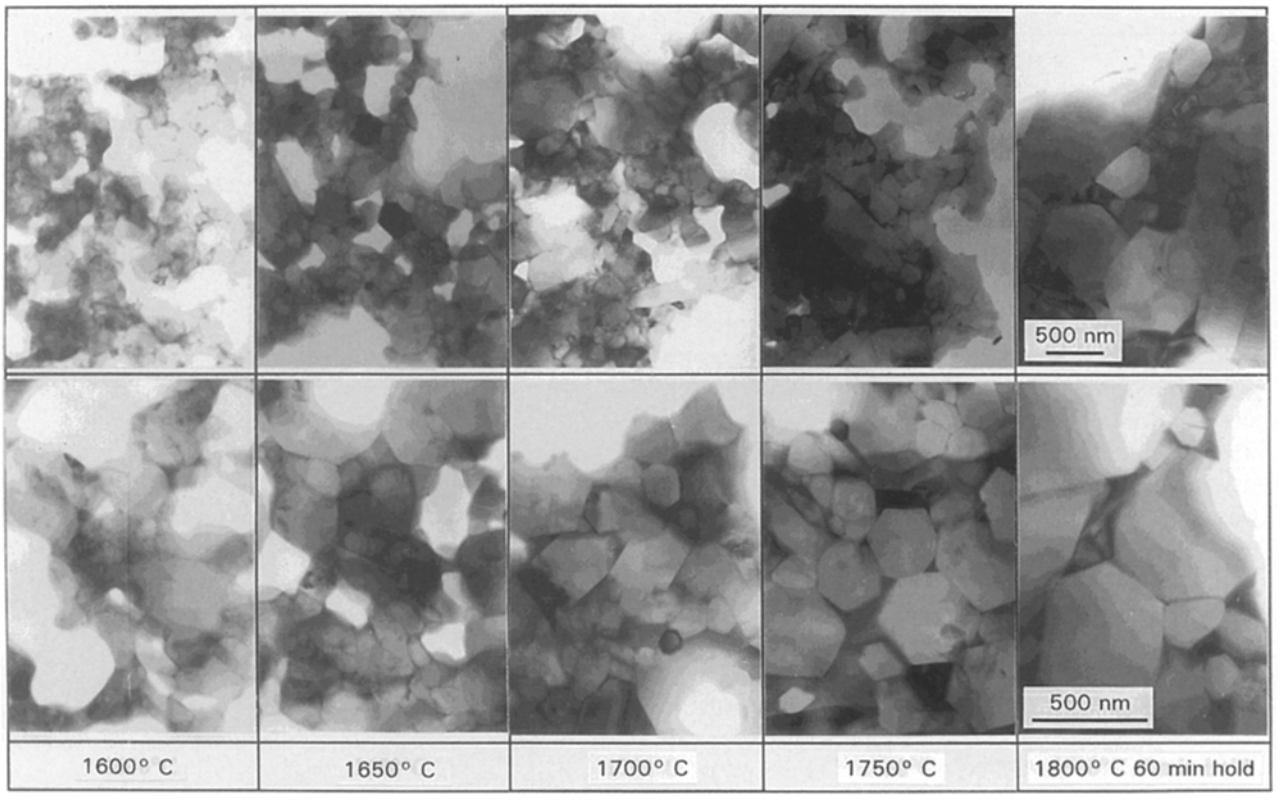

Figure 5 Transmission electron micrographs of Si_3N_4 with 10% Al_2O_3.

the additive composition were divided into two groups. The first, for Al_2O_3-rich additives, indicates that densification was completed before full transformation occurred. The second, for Y_2O_3- rich additives, shows that densification and complete transformation were achieved at nearly the same time.

3.2. Microstructure: general morphology

Figs 4 and 5 show the bright-field transmission electron micrographs indicating morphological changes with sintering temperature for the 5Y2A and the 10A additives, respectively. For both additives, the grain size did not change much in the temperature range

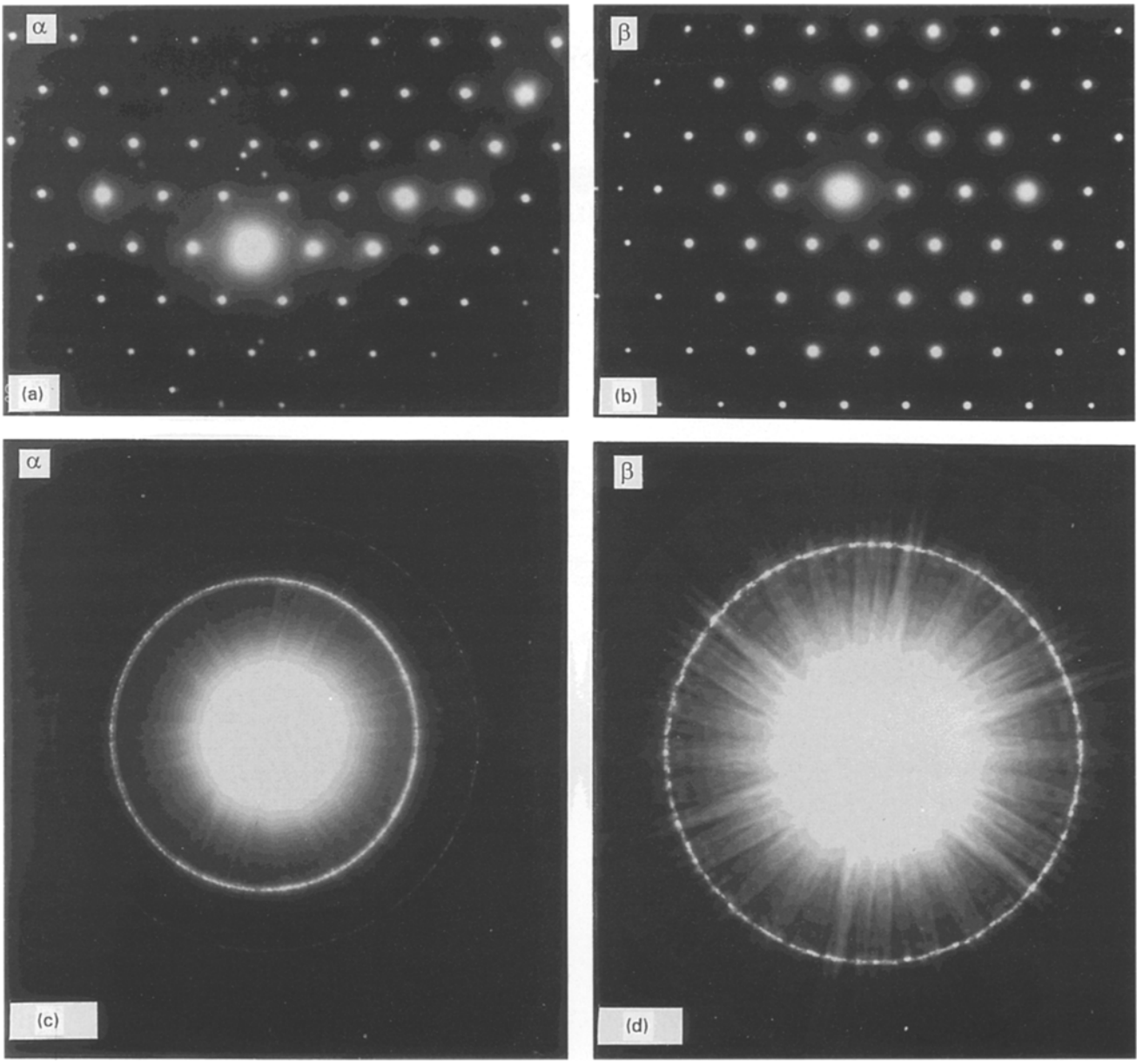

Figure 6 (a, b) Selected-area electron diffraction (SAD) patterns and (c, d) convergent beam electron diffraction (CBED) patterns for α- and β-Si_3N_4. The former do not allow α and β to be distinguished, whereas the latter do.

1600–1750 °C, but grain growth was observed in the samples hot-pressed at 1800 °C for 60 min. The grain shape changed from granular to hexagonal shape following the α–β transformation for samples with 5Y2A additive but did not change for the 10A additive. The equi-axed grain shape for the Si_3N_4 with the 10A additive was probably caused by the fact that the α–β transformation did not progress until after the completion of densification. Thus, elongation of columnar β-Si_3N_4 grains was inhibited by full densification.

3.3. Identification of α and β-Si_3N_4 by CBED

SAD patterns and CBED patterns of α- and β-Si_3N_4 are shown in Fig. 6 in the case of ⟨0 0 1⟩ beam incidence. No difference between the conventional SAD patterns was apparent, while the CBED patterns displayed clear differences between α- and β-Si_3N_4. The SAD pattern shows diffraction only from the zero-order Laue zone (ZOLZ). However, if the electron beam is converged, diffraction from the first-order Laue zone (FOLZ), the second order Laue zone (SOLZ), and higher order Laue zones (HOLZ) can be observed as rings whose spacing is dependent on the *c*-axis parameter.

Fig. 7a shows SAD patterns from other zone axis. Because these diffraction spots can be indexed for both α- and β-Si_3N_4 as shown in Fig. 7b and c, phase identification is not possible. At this beam incidence, α- and β-Si_3N_4 also have a different distance, H, between the ZOLZ and FOLZ lines indicated in Fig. 7e and f, as well as in the simple case of ⟨0 0 1⟩ beam incidence. The FOLZ ring radius, R, of α-Si_3N_4 is, therefore, different from that of β-Si_3N_4, and can be calculated from the following equation [12]

$$R = \frac{2H^{\pm}}{\lambda} L\lambda \qquad (1)$$

where L is the camera length and λ is the wavelength of the electron beam. By comparison of the R value derived from Equation 1 with the experimental value shown in Fig. 7d, the α- and β-phases could be identified. Fig. 8 shows the results of a detailed CBED analysis in the sample prepared with 5Y2A additive.

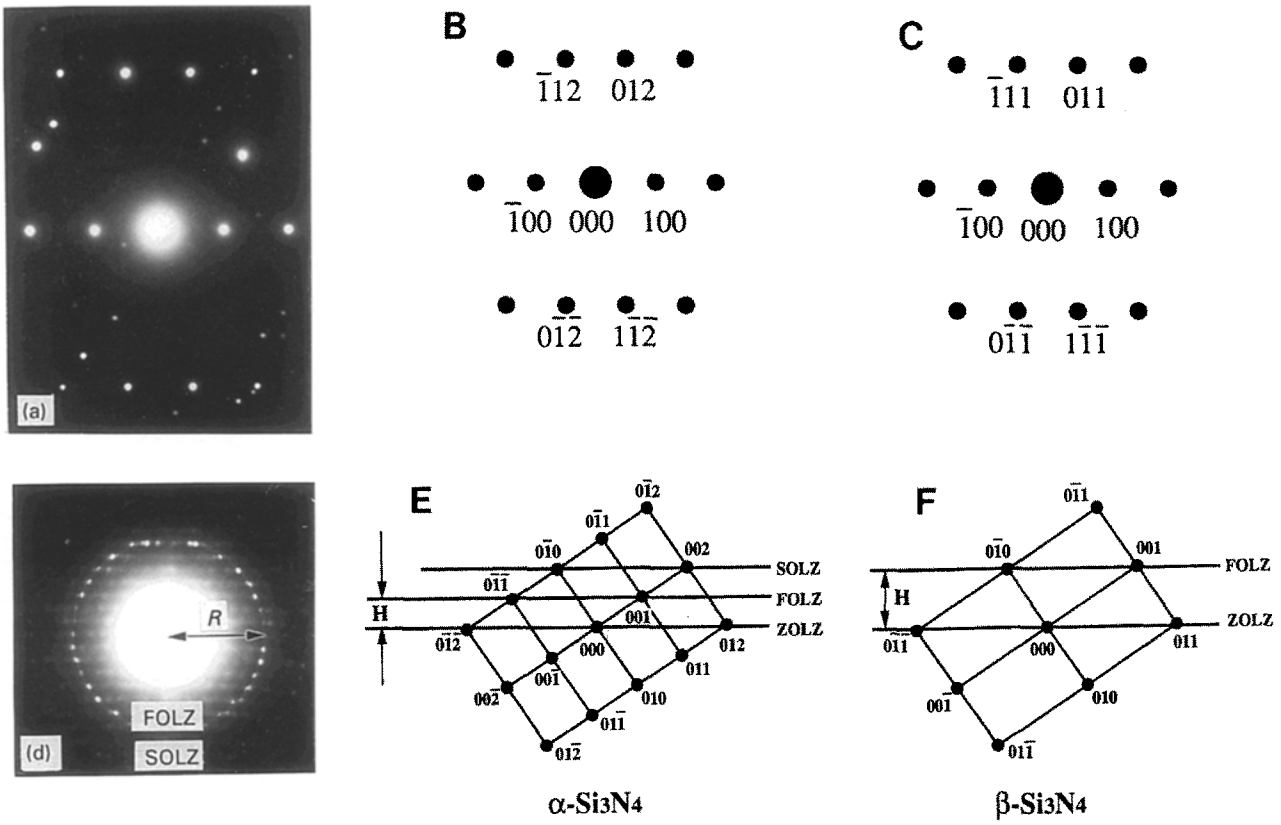

Figure 7(a–f) Electron diffraction patterns and reciprocal lattices of Si_3N_4.

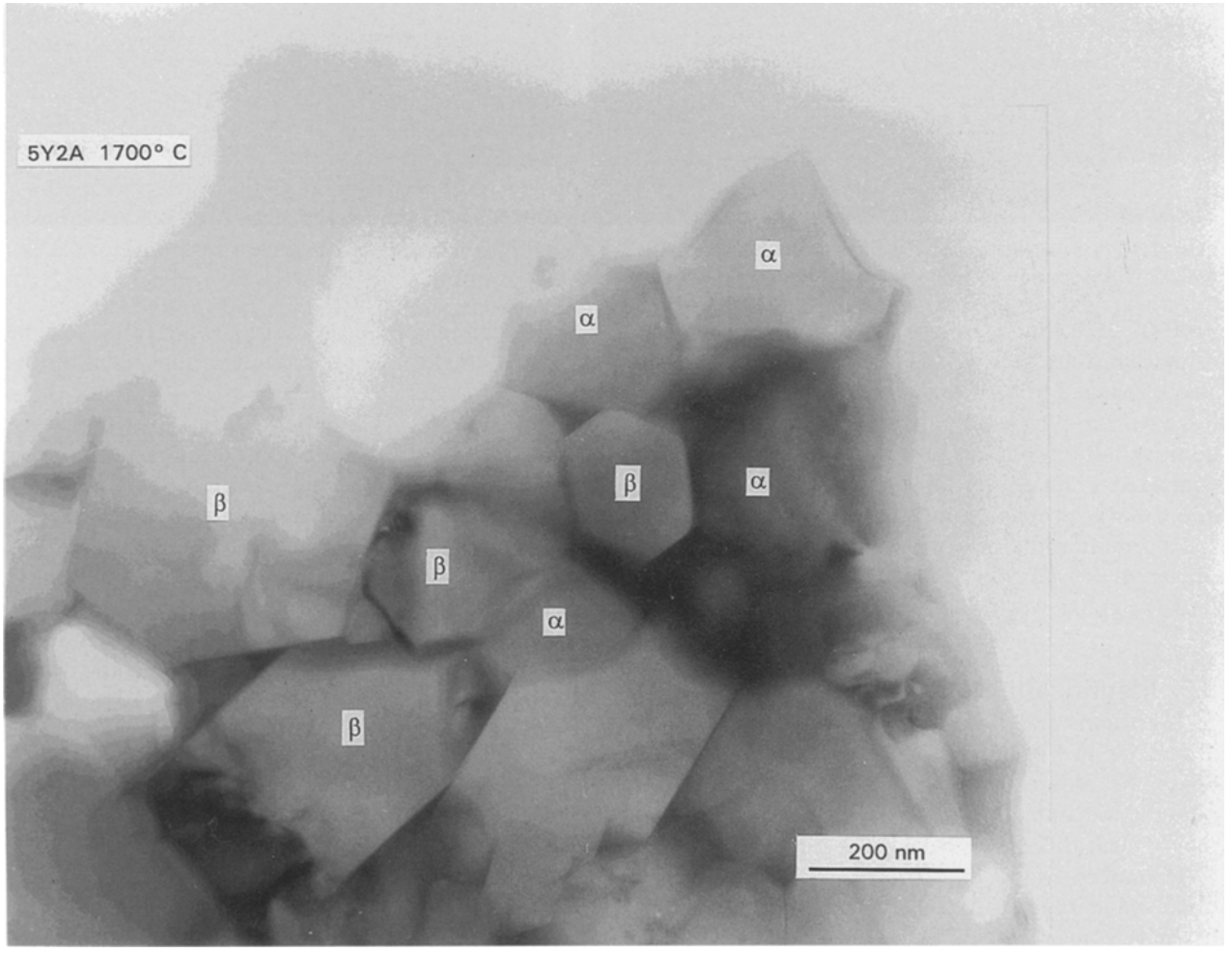

Figure 8 Transmission electron micrograph of Si_3N_4 with 5% Y_2O_3 and 2% Al_2O_3 quenched from 1700.

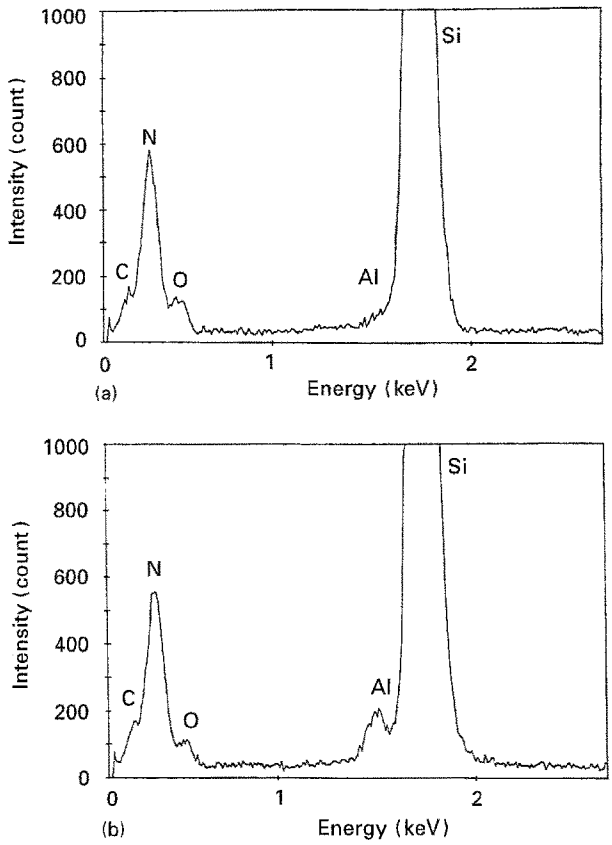

Figure 9 Typical EDS spectra of (a) α- and (b) β-Si_3N_4 (5Y2A). The carbon peak comes from the carbon-coating film of the sample.

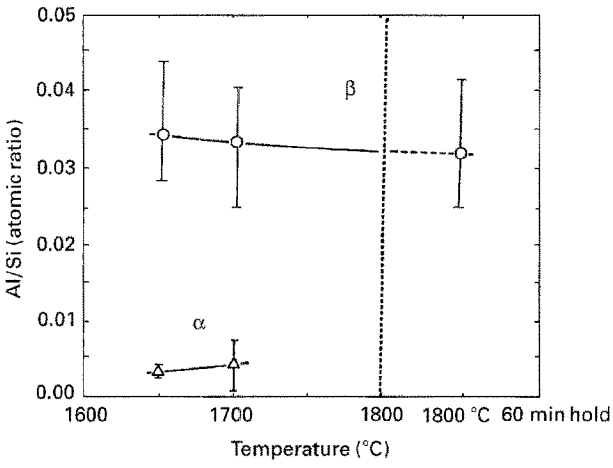

Figure 10 Variation of Al/Si atomic ratio in α- and β-Si_3N_4 grains with sintering temperature (5Y2A).

3.4. Composition analyses

The compositions of Si_3N_4 grains and grain boundaries were measured by EDS. Fig. 9 shows typical spectra from α- and β-Si_3N_4 grains for the samples with the 5Y2A additive. The aluminium peak was clearly recognized for β-Si_3N_4 grains. The results of the quantitative analysis for aluminium and silicon in the Si_3N_4 grains are shown in Fig. 10 as a function of sintering temperature for the samples with the 5Y2A additive. There is little aluminium (< 0.01 atomic ratio of Al/Si) in α-Si_3N_4, whereas β-Si_3N_4 grains contained significant amounts of aluminium (> 0.03).

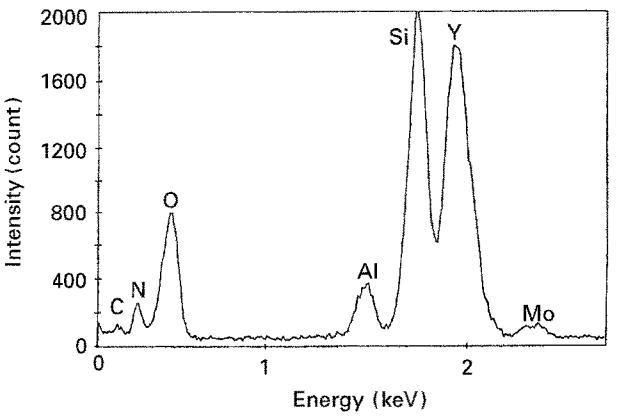

Figure 11 Typical EDS spectrum of a grain boundary in Si_3N_4 (5Y2A). The molybdenum signal comes from the specimen holder following ion milling.

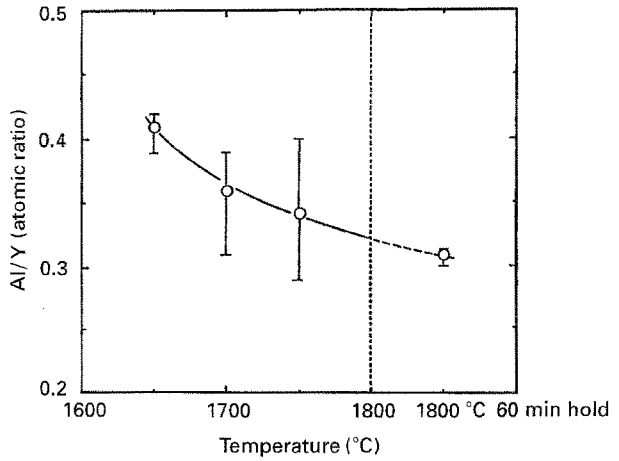

Figure 12 Variation of Al/Y atomic ratio in grain boundaries with sintering temperature (5Y2A).

This aluminium concentration did not change considerably with temperature, implying that the aluminium was incorporated into β-Si_3N_4 grains during the transformation, rather than during growth.

Fig. 11 shows a typical EDS spectrum of a grain boundary in Si_3N_4 with the 5Y2A additive. The grain-boundary compositions were quantitatively analysed and the results are shown in Fig. 12. The aluminium and oxygen concentrations were expressed as atomic ratios to yttrium, because the amount of yttrium in the grain boundaries is expected to be constant, while the X-ray intensities of silicon and nitrogen are influenced by the surrounding Si_3N_4 grains. Both Al/Y and O/Y ratios decreased with the sintering temperature. These results mean that the aluminium and oxygen concentrations in grain boundaries decreased as a result of diffusion into the Si_3N_4 grains during the α–β transformation.

The aluminium concentration in α- and β-Si_3N_4 grains of the samples with the 10A additive was also measured (Figs 13 and 14). The α-Si_3N_4 grains had only a small amount of aluminium (< 0.02 atomic ratio of Al/Si), whereas the β-Si_3N_4 grains contained a large amount of aluminium (> 0.02). This means that most of the aluminium was incorporated into the

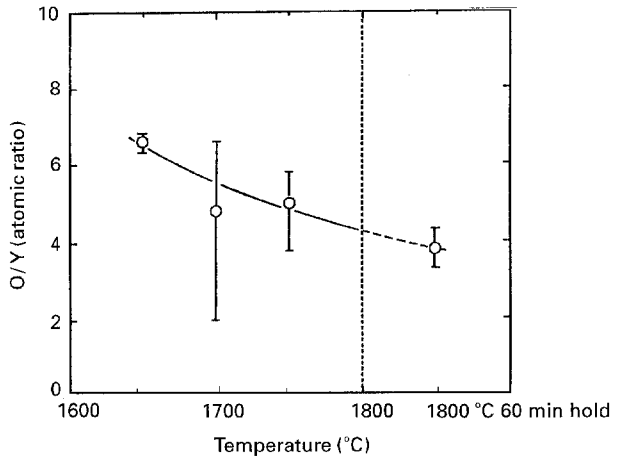

Figure 13 Variation of O/Y atomic ratio in grain-boundaries with sintering temperature (5Y2A).

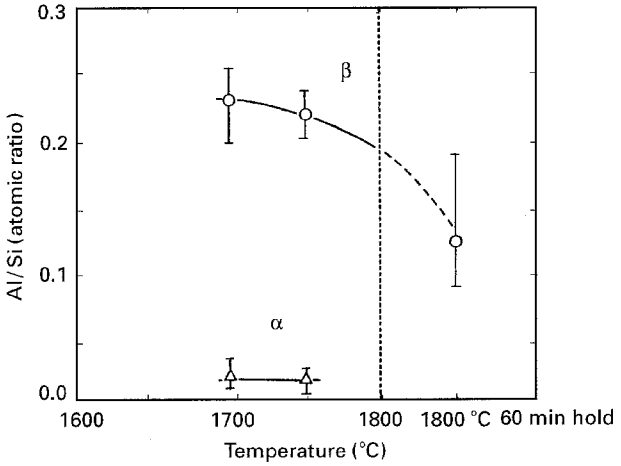

Figure 14 Variation of Al/Si atomic ratio in α- and β-Si_3N_4 grains with sintering temperature (10 A).

Si_3N_4 grains during transformation. The aluminium concentration in β-Si_3N_4 of the sample hot-pressed at 1800 °C for 60 min was lower than that of the samples at lower temperatures. It is thought that a large amount of aluminium is incorporated into the grains during the early stages of transformation. In the later stage, the aluminium concentration in grain boundaries decreased and solution of aluminium into Si_3N_4 grains decreased. During holding at 1800 °C, aluminium migrated from aluminium-rich grains to aluminium-poor grains. The difference of aluminium migration behaviour during the heating process between the sintering additives of 5Y2A and 10A is probably related to the presence of yttrium in grain boundaries.

4. Conclusions

The following conclusions may be made from the results of this investigation.

1. CBED techniques are efficient methods to differentiate between individual grains of α- and β-Si_3N_4.

2. Densification of α-Si_3N_4 with Al_2O_3-rich additives was completed before full β-phase transformation had occurred. In the case of Si_3N_4 with Y_2O_3-rich additives, densification and complete α–β transformation were achieved at nearly the same time.

3. Samples with 5Y2A and 10A additives showed grain growth after completion of transformation and densification. Si_3N_4 grains in the sample with the 5Y2A additive exhibited predominantly hexagonal shapes following transformation.

4. Most of the dissolved aluminium in Si_3N_4 was incorporated within β-grains during the transformation. The aluminium concentration in β-grains of Si_3N_4 with the 5Y2A additive was relatively constant, but that of Si_3N_4 with the 10A additive decreased with temperature and holding time.

5. The concentration of aluminium and oxygen in the grain boundary of Si_3N_4 with the 5Y2A additive decreased as the α–β phase transformation progressed.

Acknowledgements

We thank Dr M. Chandramouli, University of California at Berkeley, for helpful discussions on CBED techniques, and Mr C. J. Echer, National Center for Electron Microscopy, Lawrence Berkeley Laboratory, for assistance with analytical electron microscopy. This work was supported by the Director, Office of Energy Research, Office of Basic Energy Science, Materials Sciences Division of the US Department of Energy, under Contract DE-AC03-76SF00098.

References

1. A. R. BAKER, D. J. DAWSON and D. C. EVANS, *Mater. Design* **8** (1987) 315.
2. G. ZIEGLER, J. HEINRICH and G. WÖTTING, *J. Mater. Sci.* **22** (1987) 3041.
3. J. WEISS, *Ann. Rev. Mater. Sci.* **11** (1981) 381.
4. K. H. JACK, *J. Mater. Sci.* **11** (1976) 1135.
5. M. K. CINIBULK, GARETH THOMAS and S. M. JOHNSON, *J. Amer. Ceram. Soc.* **73** (1990) 1606.
6. *Idem, ibid.* **75** (1991) 2044.
7. K. KOMEYA, M. KOMATSU, T. KAMEDA, Y. GOTO and A. TSUGE, *J. Mater. Sci.* **26** (1991) 5513.
8. A. TSUGE and K. NISHIDA, *Am. Ceram. Sco. Bull.* **57** (1977) 424.
9. F. F. LANGE, *J. Amer. Ceram. Soc.* **62** (1979) 428.
10. K. SUZUKI and Y. KANNO, *J. Ceram. Soc. Jpn* **92** (1984) 101.
11. K. M. KRISHNAN and C. J. ECHER, in "Analytical Electron Microscopy-1987", edited by D. C. Joy (San Francisco Press, San Francisco, CA, 1987) p. 99.
12. G. THOMAS, *Ultramicroscopy* **20** (1986) 239.
13. M. TANAKA, *Bull. Jpn Inst. Metals* **28** (1989) 220.
14. J. W. STEEDS, in "Introduction to Analytical Electron Microscopy", edited by J. J. Hren, J. J. Goldstein and D. C. Joy (Plenum Press, New York, NY, 1979) p. 403.

Received 15 June
and accepted 16 September 1994